PHYSICAL REVIEW D **89,** 055015 (2014)

Viability of thermal well-tempered dark matter in SUSY GUTs

Archana Anandakrishnan[1] and Kuver Sinha[2]

[1]*Department of Physics, The Ohio State University, 191 West Woodruff Avenue, Columbus, Ohio 43210, USA*

[2]*Department of Physics, Syracuse University, Syracuse, New York 13244, USA*

(Received 12 November 2013; published 17 March 2014)

In a scenario with heavy supersymmetric sfermions and decoupled supersymmetric Higgs sector, a well-tempered neutralino is the remaining candidate for thermal single-component sub-TeV dark matter. Well-tempered neutralinos are studied in the context of supersymmetric grand unified theories (GUTs) with third family Yukawa coupling unification. A global χ^2 analysis is performed, including the observables M_W, M_Z, G_F, $\alpha_{\rm em}^{-1}$, $\alpha_s(M_Z)$, M_t, $m_b(m_b)$, M_τ, $b \to s\gamma$, BR$(B_s \to \mu^+\mu^-)$, M_h and Ωh^2. Tensions in simultaneously fitting the Higgs and bottom quark masses while also avoiding gluino mass bounds from the LHC disfavors light Higgsinos with mass $\lesssim$500 GeV, ruling out light bino/Higgsino dark matter candidates. Bino/wino/Higgsino and bino/wino candidates fare somewhat better although they are fine-tuned and require departure from GUT-scale gaugino mass universality (the example chosen here is the mixed modulus-anomaly pattern). Implications for dark matter direct detection of these models as well as collider signatures are briefly discussed. Independent of the thermal dark matter viability, these models will be severely constrained by the absence of a gluino at the next run of LHC.

DOI: 10.1103/PhysRevD.89.055015 PACS numbers: 12.60.Jv, 12.10.-g

I. INTRODUCTION

The major motivations for supersymmetric extensions of the Standard Model (SM) are gauge coupling unification, a solution to the hierarchy problem, and the existence (in R-parity conserving models) of a dark matter (DM) candidate. In particular, supersymmetry allows the gauge couplings to unify at an amazing precision of about 3% [1–6]. Supersymmetric grand unified theories (SUSY GUTs) also allow for Yukawa coupling unification. For example, in minimal SO(10) GUTS, each family of the Standard Model matter lives in one **16**-dimensional representation, while the Higgses live in a **10**-dimensional representation. The only renormalizable Yukawa coupling that can be written down in such theories is a λ **16 10 16**, allowing for Yukawa coupling unification at the GUT scale. $t-b-\tau$ Yukawa unification requires $\tan\beta \simeq 50$ in order to reproduce the correct ratio between the top and the bottom quark masses. The constraints on the SUSY boundary conditions at the GUT scale coming from requiring Yukawa unification have been extensively studied [7–17].

In SUSY GUT models with universal gaugino masses at the GUT scale, the lightest supersymmetric particle (LSP) is typically a pure bino, for which the DM relic density is too high in thermal histories.[1] A pure thermal bino could produce the observed relic density through coannihilation effects or the A resonance, in a region where $M_A \sim 2m_{\tilde{\chi}_1^0}$, where M_A is the mass of the pseudoscalar Higgs. Neither of these options are straightforward, however. Since each SM generation belongs to a **16**-dimensional representation there is one universal scalar mass for each family at the GUT scale. The third-generation sfermion mass is constrained to be very heavy ($\gtrsim$few TeV) due to flavor physics constraints from $b \to s\gamma$ transitions that are enhanced at large $\tan\beta$. Hence, coannihilation effects due to a light slepton that is nearly mass degenerate with the LSP are difficult to obtain in these SUSY GUTs (assuming that the DM mass is itself in the sub-TeV range). Moreover, Yukawa unified GUTs prefer a large CP-odd Higgs mass to satisfy the $B_s \to \mu^+\mu^-$ constraint which puts the A-resonance region also in tension. The popular remaining options are to opt for a candidate such as the pure wino or Higgsino (either in a nonthermal setting [21] or as a part of multicomponent DM scenarios [22,23]) or to rely on a (thermal) well-tempered candidate. We will not explore the nonthermal or multicomponent options in this paper. Dark matter in Yukawa unified SUSY GUTs have been discussed in earlier works of Refs. [23–26].

The purpose of this paper is to study thermal, single-component well-tempered DM candidates [27] satisfying the relic density in SUSY GUT models, given the constraints emerging from the Large Hadron Collider (LHC). For models with heavy scalars, the gluino is constrained by CMS and ATLAS searches [28,29] to be $M_{\tilde{g}} \gtrsim$ 1–1.2 TeV, where the actual bound depends on the search strategy based on the final states from the decay of the gluino. On the other hand, the LHC has observed a new boson consistent with the SM Higgs with mass of about 125 GeV [30,31].

[1]We note that nonthermal histories with a bino LSP can satisfy the relic density if it is produced from the decay of a modulus with just the correct density and undergoes no further annihilation. This scenario, called the "branching scenario," has been studied in [18–20].

One of the first conclusions we draw from the current study is that light [$\lesssim \mathcal{O}(500)$ GeV] Higgsinos are difficult to obtain in Yukawa unified SUSY GUT models. This comes from simultaneously satisfying the observed Higgs mass and corrections to the bottom quark mass while also obtaining a gluino heavier than the LHC-excluded lower bound. For gluino $\gtrsim 1.2$ TeV, we find tensions in obtaining a 125 GeV Higgs mass, in spite of the heavy scalars. The fact that light Higgsinos are difficult to obtain implies that light bino/Higgsino ($\tilde{B}/\tilde{H}$) DM is disfavored in these models. This further implies that universal gaugino mass conditions, where $\tilde{B}/\tilde{H}$ is the only viable thermal well-tempered DM candidate (due to large mass separation between the bino and the wino), are similarly disfavored.

We then proceed to explore bino/wino/Higgsino ($\tilde{B}/\tilde{H}/\tilde{W}$) and bino/wino DM ($\tilde{B}/\tilde{W}$). These cases require departure from gaugino mass universality at the GUT scale (to reduce the mass separation between bino and wino). The boundary condition we choose is mixed modulus-anomalous (mirage) mediation [32–34] which is independently well motivated from string constructions. We perform a global χ^2 analysis including the observables M_W, M_Z, G_F, $\alpha_{\rm em}^{-1}$, $\alpha_s(M_Z)$, M_t, $m_b(m_b)$, M_τ, $b \to s\gamma$, $BR(B_s \to \mu^+\mu^-)$ and M_h. We then explore the best fit regions and study the thermal relic abundance Ωh^2.

Our main findings for $\tilde{B}/\tilde{H}/\tilde{W}$ and $\tilde{B}/\tilde{W}$ are the following: Compared to the case of universal gaugino masses and $\tilde{B}/\tilde{H}$ DM, these cases perform better but are also somewhat fine-tuned. A certain degree of fine-tuning is expected in general for bino/wino coannihilation effects to be operational. This is exacerbated by the additional constraints on the Higgsinos, outlined above and shown in detail in Sec. III. Nevertheless, we obtain regions of parameter space that have a well-tempered neutralino DM and fit the other observables mentioned above at 90%–95% confidence level.

The best fits are obtained for a certain range of α which is a parameter that controls the degree of departure from GUT-scale gaugino universality. α parametrizes the relative importance of (universal) modulus-mediated and (β-function-dependent) anomaly-mediated contributions to the GUT-scale gaugino masses. For $\alpha \sim 0$ (the limit in which anomaly-mediated contributions vanish), the tensions associated with universal gaugino masses become manifest while for large α (the limit in which anomaly-mediated contributions dominate), the well tempering is ruined and the LSP becomes winolike. In the intermediate regions of α, the DM is a well-tempered $\tilde{B}/\tilde{H}/\tilde{W}$ or $\tilde{B}/\tilde{W}$, where each component plays a role in the final annihilation cross section. Typically, in the case of $\tilde{B}/\tilde{H}/\tilde{W}$ DM, the Higgsino component in the LSP turns out to be less than 8%, allowing us to (just) evade current direct detection limits although this type of DM will be detectable in the near future. The main annihilation channels in this region are $\tilde{\chi}_1^0\tilde{\chi}_1^0 \to Zh$ and the coannihilation channels are $\tilde{\chi}_1^0\tilde{\chi}_2^0$, $\tilde{\chi}_1^0\tilde{\chi}_1^\pm \to ZW$. In the case of $\tilde{B}/\tilde{W}$ DM, the Higgsino content is less than 1% and the relic density is mainly satisfied through coannihilation effects while the spin-independent scattering cross section is much below current direct detection bounds.

It is important to note that independent of the thermal dark matter viability, these models will be severely constrained by the absence of a gluino at the next run of LHC. The best fit regions require a light gluino. The lower bound on the gluino mass is growing from the LHC data and the 14 TeV run at the LHC will conclusively test the regions discussed here.

The plan of the paper is as follows: In Sec. II, we introduce Yukawa unified SUSY GUT models, discuss well tempering in these scenarios, and also discuss the procedure we adopt for the obtaining the best fit points. In Sec. III, we present the case light Higgsinos and bino/Higgsino DM in models with universal gaugino masses. Section IV contains our results for the $\tilde{B}/\tilde{H}/\tilde{W}$ and $\tilde{B}/\tilde{W}$ DM. Here, we first give a short background on the mirage boundary conditions and then present the spectra, fits, and properties of the well-tempered scenarios. We end with our conclusions. In the Appendixes, we present analytical expressions for the annihilation cross section of $\tilde{\chi}_1^0\tilde{\chi}_1^0 \to Zh$, which is one of the main annihilation channels of the $\tilde{B}/\tilde{H}/\tilde{W}$ case. We also show the best fit regions for several intermediate values of the parameter α, which demonstrate that the fits get progressively better as one departs from gaugino universality.

II. MODEL AND PROCEDURE

Supersymmetric parameters are heavily constrained when one requires Yukawa coupling unification. In the case of $t-b-\tau$ Yukawa unification, one Yukawa coupling gives rise to the top, bottom and the tau masses. The only way to reproduce the hierarchy between the top and the bottom masses is by requiring large $\tan\beta \sim 50$. At large $\tan\beta$, the GUT-scale SUSY parameters are further constrained. For example, in the large $\tan\beta$ regime the down quark mass matrix and the Cabibbo-Kobayashi-Maskawa matrix elements receive significant corrections [35]. Thus, requiring that the Yukawa couplings unify in addition to gauge coupling unification removes a lot of freedom from the GUT-scale parameters.

The model parameters are summarized in Table I. The model is defined by three gauge parameters, α_G, M_G, ϵ_3, where $\alpha_1(M_G) = \alpha_2(M_G) \equiv \alpha_G$, and $\epsilon_3 = \frac{\alpha_3 - \alpha_G}{\alpha_G}$ is the GUT-scale threshold corrections to the gauge couplings. There is one large Yukawa coupling, λ, such that $\lambda_t(M_G) = \lambda_b(M_G) = \lambda_\tau(M_G) = \lambda$. Typically, there are small corrections to this relation at the GUT scale, coming from the off-diagonal Yukawa couplings to the first two families. Here we consider a third family model, since the SUSY spectrum (and relic abundance) does not heavily depend on these small off-diagonal Yukawa couplings.

TABLE I. The model is defined by three gauge parameters, one large Yukawa coupling and six SUSY parameters defined at the GUT scale. The parameters μ, $\tan\beta$ are obtained at the weak scale by consistent electroweak (EW) symmetry breaking.

Sector	Third family analysis
Gauge	α_G, M_G, ϵ_3
SUSY (GUT scale)	m_{16}, $M_{1/2}$, α, A_0, m_{10}, D
Textures	λ
SUSY (EW scale)	$\tan\beta$, μ
Total number	12

SUSY parameters defined at the GUT scale include a universal scalar mass for squarks and sleptons, m_{16}; universal gaugino mass, $M_{1/2}$; m_{10}, the universal Higgs mass; A_0, universal trilinear scalar coupling and D, the magnitude of Higgs splitting.[2]Note that nonuniversal Higgs masses are necessary in order for radiative electroweak symmetry breaking in these models. We will also consider in general a parameter α that determines the ratio of anomaly mediation to gravity mediation contribution to the gaugino masses. The parameters μ, $\tan\beta$ are obtained at the weak scale by consistent electroweak symmetry breaking. In the case of $t-b-\tau$ unification, $\tan\beta$ is restricted to be around 50.[3]

We follow the same procedure used in Ref. [16] to calculate 12 low-energy observables. We use the 2-loop renormalization group equations (RGEs) for both dimensionful and dimensionless parameters, integrate out the heavy scalars at their masses, and evolve all parameters to the weak scale without the first two generation scalars. We use MATON to perform the RGE evolution, calculation of the couplings at the weak scale and the masses of the gauge bosons, top, bottom quarks and the τ lepton. For the calculation of Higgs mass, we define an effective theory at the scale $M_{\rm SUSY}$ and interface our calculation with the code by authors in Ref. [36]. The flavor observables are calculated using the code SUSY_FLAVOR [37], and the relic abundance is computed using MICROMEGAS [38]. A χ^2 function is constructed by comparing the predicted observables y_i (except the relic abundance) with their measured values $y_i^{\rm data}$, given by the standard definition

$$\chi^2 = \sum_i \frac{|y_i - y_i^{\rm data}|^2}{\sigma_i^2}, \tag{1}$$

[2]Here we study the case of "just-so" Higgs splitting, and D also fixes the magnitude of splitting for all scalar masses in the case of D-term splitting.

[3]We also considered the possibility of relaxing $t-b-\tau$ unification to $b-\tau$ unification by allowing an independent Yukawa coupling for the bottom and tau, such that $\lambda_t = \lambda_u$ and $\lambda_b = \lambda_\tau = \lambda_d$. But the fits that we obtained were consistent with $t-b-\tau$ unification to within a few percent, and the extra parameter dependence was eliminated.

TABLE II. The 12 observables that we compare in the SUSY GUT model and their experimental values. Capital letters denote pole masses. We take LHCb results into account but use the average by Ref. [40]. All experimental errors are 1σ unless otherwise indicated. Finally, the Z mass is fit precisely via a separate χ^2 function solely imposing electroweak symmetry breaking. Ωh^2 is not included in the χ^2 minimization procedure.

Observable	Exp. value	Ref.	Th. error
$\alpha_3(M_Z)$	0.1184 ± 0.0007	[41]	0.5%
$\alpha_{\rm em}$	$1/137.035999074(44)$	[41]	0.5%
G_μ	$1.16637876(7) \times 10^{-5}$ GeV^{-2}	[41]	1.0%
M_W	80.385 ± 0.015 GeV	[41]	0.5%
M_Z	91.1876 ± 0.0021	[41]	0.5%
M_t	173.5 ± 1.0 GeV	[41]	0.5%
$m_b(m_b)$	4.18 ± 0.03 GeV	[41]	0.5%
M_τ	1776.82 ± 0.16 MeV	[41]	0.5%
M_h	$125.3 \pm 0.4 \pm 0.5$ GeV	[30]	0.5%
BR$(b\to s\gamma)$	$(343 \pm 21 \pm 7)\times 10^{-6}$	[40]	(181–249) $\times 10^{-6}$
BR$(B_s\to\mu^+\mu^-)$	$(3.2 \pm 1.5) \times 10^{-9}$	[42]	(1.5–4.7) $\times 10^{-9}$
Ωh^2	0.1187 ± 0.0017	[43]	0.08–0.2

where σ_i is the assumed uncertainty in the calculation of the observable. The χ^2 function is minimized to determine the best set of GUT-scale parameters. This minimization procedure is carried out using MINUIT [39]. The input parameters are listed in Table I, and the observables and the theoretical errors assumed in estimating them are summarized in Table II. Note that the model is defined in terms of 12 parameters of which some are fixed during the minimization procedure. We compare our predictions to 11 observables and calculate the 68%, 90%, and 95% confidence level intervals using the χ^2 function for the appropriate number of degrees of freedom (d.o.f.).

The main constraints on the SUSY spectrum come from fitting the third family masses, the Higgs mass, and the flavor observables $b\to s\gamma$ and $B_s\to\mu^+\mu^-$. Fitting the $t-b-\tau$ masses requires that $\tan\beta$ be around 50, in order to reproduce the hierarchy between the top and the bottom masses, when $\lambda_t(M_G) = \lambda_b(M_G)$. In addition, fitting the bottom mass and the Higgs mass simultaneously requires light gluinos [15]. The flavor physics observable $b\to s\gamma$ is enhanced by a chargino-top squark loop at large $\tan\beta$, and requires that the top squarks (and consequently all scalars) be heavier than a few TeV. $B_s\to\mu^+\mu^-$ rate is also enhanced at large $\tan\beta$, and constrains CP-odd Higgs mass, $M_A \gtrsim 1.2$ TeV. This pushes the model to the decoupling regime ($M_A \gg M_Z$), and the lightest Higgs is predicted to be SM-like.

A. Well tempering in SUSY models

The lightest neutralino in the minimal supersymmetric standard model is a mixture of the bino ($\tilde{B}$), wino ($\tilde{W}$), and Higgsino ($\tilde{H}_1$, $\tilde{H}_2$) eigenstates

$$\tilde{\chi}_1^0 = N_{11}\tilde{B} + N_{12}\tilde{W} + N_{13}\tilde{H}_1 + N_{14}\tilde{H}_2, \quad (2)$$

where the N_{1i} are the relevant weights along the different directions.

There are essentially three options for obtaining the observed relic density: (i) Thermal single-component DM: the lightest neutralino is the sole DM candidate and the observed relic density is obtained by thermal freeze-out. (ii) Nonthermal single-component DM: the lightest neutralino is the sole DM candidate and has a nonthermal cosmological history. Both cases of thermal underproduction and overproduction can be accommodated in this case. (iii) Multicomponent DM: the relic density is satisfied by the lightest neutralino along with one or more additional candidates, motivated by other physics (not necessarily supersymmetry). We will be interested in option (i) above, reserving the study of nonthermal DM in these models for future work.

If $\tilde{\chi}_1^0$ is a pure Higgsino, i.e. $N_{11} = N_{12} = 0$, the thermal relic density is approximately given by $\Omega h^2 \sim 0.1(\frac{\mu}{1\ \mathrm{TeV}})^2$. Clearly, TeV-scale Higgsinos are required to satisfy the thermal relic density. A pure Higgsino LSP with a thermal history is thus somewhat in conflict with naturalness arguments.[4] Similarly, for a pure wino, i.e. $N_{11} = N_{13} = N_{14} \sim 0$, the thermal relic density is satisfied for masses around 2.5 TeV. A pure bino overproduces DM in the scenario considered in this paper, with decoupled supersymmetric scalar and Higgs sectors.

The correct relic density can be obtained if $\tilde{\chi}_1^0$ is an appropriate admixture of bino, wino, and Higgsino states. There are three possibilities here: a $\tilde{B}/\tilde{H}$, $\tilde{B}/\tilde{W}$, and a $\tilde{B}/\tilde{H}/\tilde{W}$ DM candidate. The idea is that an overabundant bino acquires a larger wino or Higgsino component, allowing it to annihilate rapidly to Z, W, and h final states. For the case of $\tilde{B}/\tilde{H}$ DM, the low-energy values of M_1 and μ are required to be close to each other, typically to within 10%. $\tilde{B}/\tilde{W}$ DM requires $M_1 \sim M_2$ and gives the correct relic density mainly through coannihilation of $\tilde{\chi}_1^0$ with $\tilde{\chi}_2^0$ and $\tilde{\chi}_1^\pm$.

III. LIGHT HIGGSINOS AND $\tilde{B}/\tilde{H}$ DM WITH UNIVERSAL GAUGINO MASSES

In this section, we discuss the case of well-tempered DM in Yukawa unified SUSY GUTs with universal gaugino masses. Since $\tilde{B}/\tilde{W}$ DM requires $M_1 \sim M_2$ at low energies, it cannot be obtained if one assumes gaugino unification at the GUT scale. The remaining option then is $\tilde{B}/\tilde{H}$ DM. This requires light Higgsinos. There is, however, a very strong tension in obtaining $\tilde{B}/\tilde{H}$ DM in these models. This tension arises from an unusual candidate: the corrections to the bottom quark mass.

It is well known that there are corrections to the bottom quark mass from a gluino-sbottom loop and a chargino-top squark loop in that are $\mathcal{O}(\tan\beta)$ enhanced. These large corrections can be written as

$$\frac{\delta m_b}{m_b} \simeq \frac{g_3^2}{12\pi^2}\frac{\mu M_{\tilde{g}}\tan\beta}{m_{\tilde{b}}^2} + \frac{\lambda_t^2}{32\pi^2}\frac{\mu A_t \tan\beta}{m_{\tilde{t}}^2}, \quad (3)$$

where $m_{\tilde{b}}$, $m_{\tilde{t}}$ and $M_{\tilde{g}}$ are the sbottom, top squark, and gluino masses, respectively. When the top squark and sbottom masses are roughly degenerate $\sim\tilde{m}$, we can rewrite the above expression as

$$\frac{\delta m_b}{m_b} \simeq \frac{\mu\tan\beta}{\tilde{m}^2}\left(\frac{g_3^2}{12\pi^2}M_{\tilde{g}} + \frac{\lambda_t^2}{32\pi^2}A_t\right). \quad (4)$$

Light Higgsinos (small μ) suppresses these corrections, which have to be at about a few percent (and negative), and are necessary to fit the bottom quark mass. This requirement places stringent constraints on the SUSY boundary conditions in the large $\tan\beta$ regime. When the scalars are heavy, and when μ is small, one needs percent level fine-tuning between the gluino mass, $M_{\tilde{g}}$ and the A_t parameter to generate these corrections. Collider constraints from LHC place significant lower bounds on the gluino mass, which is required to be heavier than $\sim$1000 GeV in these models. Therefore, to get the correct $\sim$few percent corrections, the trilinear coupling has to be large (and negative). When the absolute value of the trilinear coupling is forced to be larger than $\sim\sqrt{6}\tilde{m}$ (maximal mixing), it drives the Higgs mass to smaller values (or equivalently, the bad fit can be transferred to the bottom and tau mass). This tension between the bottom quark mass and the Higgs mass disfavors light Higgsinos in these models.

This tension is reinforced further when one considers well tempering in this context. If one does take the Higgsinos with mass $\sim$400 GeV or greater, binos are constrained to have similar mass, to give a well-tempered DM. Because of gaugino universality, the gluinos then have mass $\sim$1300–2000 GeV (but cannot be too much lighter), further forcing trilinear terms to go beyond maximal mixing. These tensions are reflected in Fig. 1 with universal gaugino masses at the GUT scale, where the best fit points are displayed in the $M_{1/2}$–μ plane. The region between the red lines has relic density in the range $\Omega h^2 = 0.08$–0.2. The relic abundance is satisfied in this region due to a well tempering of bino/Higgsino DM (due to universal conditions, the bino-wino mass splitting is too large to allow coannihilation). The olive curves are contours of constant gluino mass. In the plot, the regions under the blue contours (lightest to darkest) represent $\chi^2/\mathrm{d.o.f.} = 1.2,\ 2.3,\ 3$ corresponding to 68%, 90%, and 95% C.L., respectively. The regions were obtained by a parameter space scan with 2

[4]Naturalness arguments generally make the prediction of a small μ term: since the mass of the Z is set by the relation $m_Z^2 = \mu^2 + m_{H_u}^2$ (in the large $\tan\beta$ limit), small fine-tuning requires $\mu \sim m_Z$.

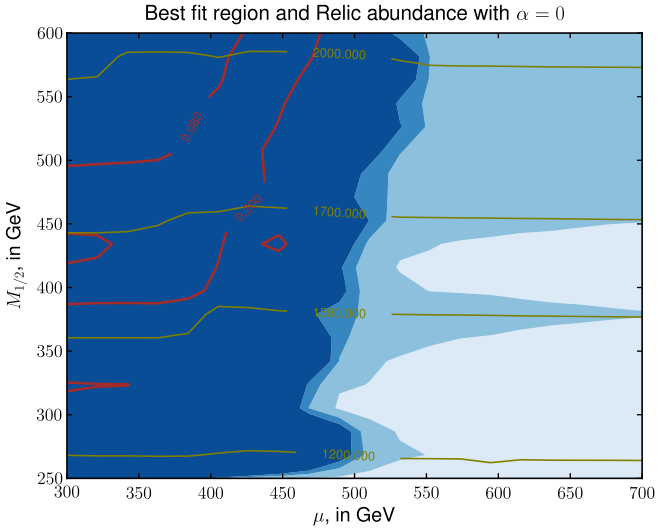

FIG. 1 (color online). Universal gaugino masses and $\tilde{B}/\tilde{H}$ DM: Best fit regions on a graph of $M_{1/2}$ versus μ in the case of $\alpha = 0$ (universal gaugino masses). The region between the red lines gives $\Omega h^2 = 0.08$–0.2, and the DM in this region is a well-tempered $\tilde{B}/\tilde{H}$. The olive curves are contours of constant gluino masses. The blue contour regions (lightest to darkest) represent the best fit regions at 68%, 90%, and 95% C.L., respectively. Note that light Higgsinos (and hence light $\tilde{B}/\tilde{H}$ DM) are not preferred.

degrees of freedom (m_{16}, μ, and $M_{1/2}$ were held fixed). Well tempering is obtained for comparable bino and Higgsino masses, which gives gluinos in the mass range of 1600–2000 GeV. The situation is worse for pure Higgsino DM which have to be heavier than a TeV and thus requiring even heavier gauginos. Therefore, in comparison with the phenomenological scenarios of C and nonuniversal Higgs masses (NUHM), Yukawa unified GUTs are further constrained. Note that in the case of C and NUHM it has been pointed out that a TeV-scale Higgsino LSP is preferred since it is unconstrained by current experiments and the correct Higgs mass can be easily obtained in this region [44,45].

We find from our χ^2 analysis that in this case, the worst fits are to $m_b(m_b)$, and M_τ, and α_s all of which have pulls $\gg 1$. It is also clear from Fig. 1 that regions with $\mu \lesssim \mathcal{O}(500)$ GeV generally give large $\chi^2/\text{d.o.f.} > 3$ in these scenarios. It is abundantly clear that there is tension between requiring Yukawa unification and a well-tempered DM, when one starts with universal gaugino masses. To retain the thermal single-component DM scenario in these models, one must move away from the gaugino mass unification assumption at the GUT scale.

IV. $\tilde{B}/\tilde{H}/\tilde{W}$ AND $\tilde{B}/\tilde{W}$ DM

In this section, we relax gaugino mass universality at the GUT scale to add the possibility of having $\tilde{B}/\tilde{H}/\tilde{W}$ or $\tilde{B}/\tilde{W}$ DM candidates. A particularly well-motivated boundary condition is combining a universal (modulus) contribution with varying degrees of anomaly-mediated contributions. To this end, we first give some basic details about mixed modulus-anomaly or mirage mediation. We then give our main results for $\tilde{B}/\tilde{H}/\tilde{W}$ and $\tilde{B}/\tilde{W}$ DM.

A. Effective mirage mediation

Nonuniversal gaugino masses could arise when there is a nonsinglet F term under the GUT symmetry or when there are hybrid SUSY breaking mechanisms. States in nonsinglet representations of the gauge symmetry could contribute large threshold corrections to the gauge couplings and could ruin precision gauge coupling unification. Hence we depart from gaugino universality by assuming that there is a hybrid SUSY breaking mechanism at the GUT scale like the "mirage" mediation scenarios studied in string-inspired effective supergravity models [32–34]. The boundary conditions considered here have been recently studied within Yukawa unified SUSY GUTs [16]. Nonuniversal gaugino mass scenarios were considered in the context of GUTs in the analyses of Refs. [12–14,17,46], where the SUSY breaking F term that couples to the gaugino transforms as a nonsinglet of the unified SO(10) gauge group and hence gives rise to nonuniversal masses.

The gaugino masses at the GUT scale obey a mirage pattern:

$$M_i = \left(1 + \frac{g_G^2 b_i \alpha}{16\pi^2} \log\left(\frac{M_{\rm Pl}}{m_{16}}\right)\right) M_{1/2}. \tag{5}$$

In the above expression, α is a parameter that controls the relative importance of the universal and anomalous contributions, and $b_i = (33/5, 1, -3)$ for $i = 1, 2, 3$ are the relevant β-function coefficients. We note that larger α leads to larger anomaly-mediated contributions (and hence departure from the universal scenarios). The definition of α has appeared in different forms in the literature. The above expression matches with the definition in Ref. [32] (with the assumption, however, that $m_{3/2} \simeq m_{16}$) but is related to the definition in Ref. [33] by the transformation $\frac{1}{\rho} = \frac{\alpha}{16\pi^2} \ln \frac{M_{PL}}{m_{16}}$. For the scalars, we assume a universal mass and trilinear coupling at the GUT scale. Note that, while the gaugino and scalar soft terms can be obtained from the heterotic framework of Ref. [33], the issue of obtaining large A terms is still a model-building challenge. Here, we let the phenomenology guide our choice of large trilinears at the GUT scale.

The additional degree of freedom α allows well tempering by tuning the ratios of M_1 and M_2. To limit the regions of interest, we illustrate in Fig. 2 the ratio of M_1 and M_2 and the value of M_3 obtained at the weak scale by a simple 1-loop analysis. We are interested in the regions where $|M_1| \leq |M_2|$, when the lightest neutralino starts to be a blend of bino and wino. This ratio of $|M_1|$ and $|M_2|$ is obtained when α is less than 3, below which the wino becomes significantly lighter. Figure. 2 also shows that

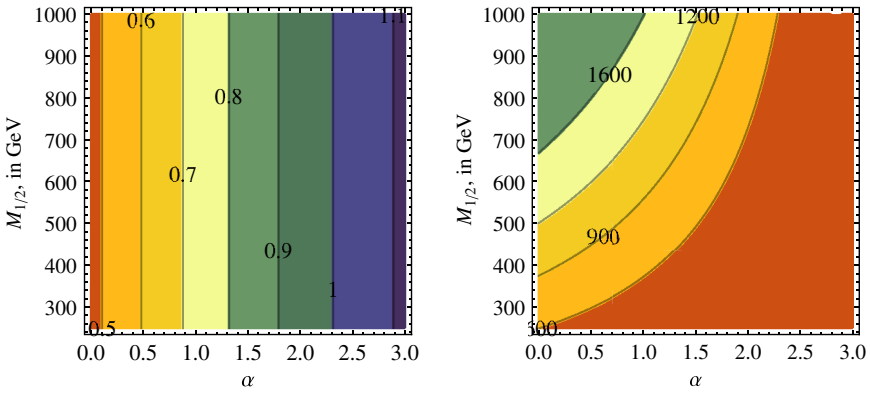

FIG. 2 (color online). The figure illustrates the relation between the gaugino masses at weak scale and the two GUT-scale parameters, $M_{1/2}$ and α using simple tree level relations. Left: The ratio of the gaugino masses M_1/M_2 at the weak scale. Right: The gluino mass parameter M_3 at the weak scale.

simultaneously satisfying the collider bound on the gluino mass further restricts $M_{1/2} > 250$ GeV. Note that the plot shows M_3 and there are additional corrections to the gluino pole mass. Once we identify the region of interest in the $M_{1/2} - \alpha$ parameter space we proceed to check if this region of the effective mirage mediation model is compatible with Yukawa unification. As an aside, we note that in Ref. [16], it was assumed that $\mu, M_{1/2} < 0$, and $\alpha \geq 4$ such that $M_3 > 0$, $M_1, M_2 < 0$. This combination was useful to simultaneously satisfy the $b \to s\gamma$ constraint and the corrections to bottom quark mass. These boundary conditions led to very distinct spectrum and interesting phenomenology but as noted earlier, large values of α lead to anomaly mediation being the dominant source of SUSY breaking, and thus a pure winolike LSP. Therefore, they are outside the range of this work on thermal single-component dark matter.

As α is gradually increased from 0, there are two important effects that become apparent. The first one is that the wino component of the LSP begins to increase. Therefore, the correct relic density is obtained for larger values of μ (compared to the universal case). Because of the constraints on light Higgsinos, this is preferable. On the other hand, since the beta-function coefficient is negative for SU(3), the gluino mass decreases with increasing α. Then the model starts conflicting with the LHC results as α increases. Below are our results for the case of $\alpha = 1.5$ in (5). In Appendix B, we discuss the intermediate values of $\alpha = 0.5$ and $\alpha = 1$, where we find progressively improving (compared to the $\alpha = 0$ case) results for the χ^2 fit. There, we also show that the model starts to conflict severely with the LHC results at around $\alpha \sim 2$. There is a finite volume of parameter space that permits well tempering and the entire volume is within the reach of the LHC and DM experiments.

B. Results for $\tilde{B}/\tilde{H}/\tilde{W}$ DM

The gaugino masses are maximally split in the universal case. As anomaly contributions increase with increasing α, the mass splitting between the gaugino masses decrease. Because of the greater proximity of bino and wino masses, now, in fact, $\tilde{B}/\tilde{H}/\tilde{W}$ and $\tilde{B}/\tilde{W}$ DM can both be options for the well-tempered DM candidate. Moreover, for the same bino mass, the gluino can now be lighter ($\gtrsim$1100 GeV), reducing the tension with fitting the b mass. Indeed, we find now that we find better fits to all the observables in Table II. This is reflected in Fig. 3, where we present fits with $\alpha = 1.5$. The region between the blue and red lines gives $\Omega h^2 = 0.08$–0.2. We see that this region now extends to

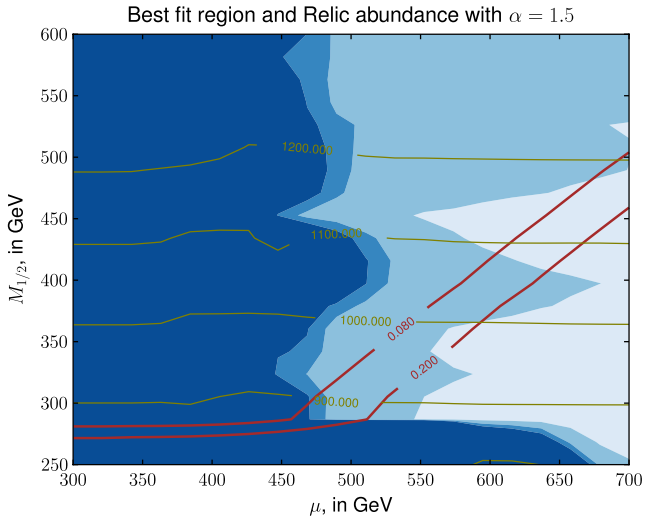

FIG. 3 (color online). $\tilde{B}/\tilde{H}/\tilde{W}$ DM: Best fit regions on a graph of $M_{1/2}$ versus μ in the case of $\alpha = 1.5$. The region between the red lines gives $\Omega h^2 = 0.08$–0.2, and the LSP in this region is a bino/wino/Higgsino admixture. The olive contours of constant gluino masses show that the gluino is lighter compared to the universal gaugino mass scenario. The blue contour regions (lightest to darkest) represent the best fit regions at 68%, 90%, and 95% C.L., respectively. The lightest blue corridor bounded by the relic density constraints is ruled out by recent direct detection exclusion bounds from LUX. Higher values of ($M_{1/2}$, μ), with heavier bino/wino/Higgsino DM, would still be allowed.

TABLE III. Spectrum at the benchmark point for $\tilde{B}/\tilde{H}/\tilde{W}$ DM.

GUT scale parameters	m_{16}	20 000	$M_{1/2}$	450	A_0	−40461	α	1.5
	m_{H_d}	27 495			m_{H_u}	23 748		
	$1/\alpha_G$	26.17	M_G	2.13×10^{16}	ϵ_3	0	λ	0.59
EW parameters	μ	660			$\tan\beta$	49.75		
Fit	Total χ^2	1.84						
Spectrum	$m_{\tilde{u}}$	∼20000	$m_{\tilde{d}}$	∼20000	$m_{\tilde{e}}$	∼20000		
	$m_{\tilde{t}_1}$	3612	$m_{\tilde{b}_1}$	5053	$m_{\tilde{\tau}_1}$	6867	$M_{\tilde{g}}$	1130
	$m_{\tilde{\chi}_1^0}$	474.5	$m_{\tilde{\chi}_2^0}$	556.7	$m_{\tilde{\chi}_3^0}$	693.6	$m_{\tilde{\chi}_4^0}$	662.9
	$m_{\tilde{\chi}_1^+}$	554.9			$m_{\tilde{\chi}_1^+}$	691.5		
	M_A	1915.3	$M_H^\pm$	1916.9	M_H	1932.5	M_h	121
DM	Ωh^2	0.121						
Gluino branching fractions	$tb\tilde{\chi}_2^\pm$	19%	$tb\tilde{\chi}_1^\pm$	17%	$g\tilde{\chi}_4^0$	17%	$t\bar{t}\tilde{\chi}_4^0$	13%
	$g\tilde{\chi}_3^0$	12%	$t\bar{t}\tilde{\chi}_2^0$	9%	$t\bar{t}\tilde{\chi}_3^0$	5%	$g\tilde{\chi}_2^0$	4%

areas of smaller χ^2, with gluino mass ∼1100 GeV. As in the universal case $\alpha = 0$, the region with low $\mu \lesssim 450$ GeV gives a large value of χ^2 and this region is qualitatively similar to the universal case. However, with larger $\mu \gtrsim 600$ GeV a region of low χ^2 opens up and the relic density band extends into it.

We present a sample benchmark point in Table III. The best fit point obtained here is very similar to the benchmark points discussed in the Dermisek-Raby model with universal gaugino masses [15]. Note that both our benchmark points prefer the value of $\epsilon_3 = 0$. ϵ_3 is the GUT-scale threshold corrections required to the fit the value of $\alpha_s(MZ)$. While standard scenarios with universal gaugino mass prefer $\epsilon_3 = -3\%$, it was shown in [47] that precision gauge coupling unification can be achieved in models with nonuniversal gaugino masses, especially with the mirage pattern with lighter gluinos considered in this work.

The SUSY boundary conditions at the GUT scale are

$$m_{16} > \text{few Tev}; \qquad m_{10} \sim \sqrt{2} m_{16};$$
$$A_0 \sim -2 m_{16}; \qquad \mu, M_{1/2} \ll m_{16}; \qquad \tan\beta \sim 50.$$

The first two families of scalars are very heavy (∼20 TeV), and the spectrum has the inverted scalar mass hierarchy with the third family of squarks and sleptons between 3 and 6 TeV. These scalars are out of the reach of the LHC. The gauginos are light and the LSP (the DM candidate) is a well-tempered $\tilde{B}/\tilde{H}/\tilde{W}$ mixture. The gaugino sector differs from the previous studies, and we are able to satisfy the relic abundance. The gluino tends to be lighter than the universal case due to the presence of the anomaly contribution. We have increased the overall scale of the gauginos, and the LSP mass but the gluino remains light enough to contribute the required corrections to the bottom quark mass. Note that all the extra Higgses of SUSY are heavy and thus the lightest Higgs is purely SM-like. In Sec. V, we will discuss the implications of current bounds from the LHC on the SUSY spectrum.

C. $\tilde{B}/\tilde{H}/\tilde{W}$ DM annihilation and scattering cross sections

The main annihilation channels of $\tilde{\chi}_1^0$ in this region are displayed in Fig. 4.

The left panel shows the annihilation cross section $\tilde{\chi}_1^0\tilde{\chi}_1^0 \to Zh$ as a function of the relic density in the zero velocity limit. The cross section is enhanced for large bino/Higgsino mixing. As the Higgsino becomes decoupled, the cross section for this annihilation channel becomes negligible. These results have been obtained using MicrOmegas and we have verified the result theoretically; the main formulas are collected in Appendix A. The right panel shows the relative importance at DM freeze-out of the $Zh + t\bar{t}$ channel and the ZW channel as a function of the relic density. For low relic density, the coannihilation channels $\tilde{\chi}_1^0\tilde{\chi}_2^0$, $\tilde{\chi}_1^0\tilde{\chi}_1^\pm \to ZW$ dominate. The DM is then a bino/wino well-tempered neutralino. For larger separation between bino and wino, the coannihilation becomes ineffective and the relic density increases as $\tilde{\chi}_1^0$ becomes predominantly bino. The main annihilation channel then becomes $\tilde{\chi}_1^0\tilde{\chi}_1^0 \to t\bar{t}$. We note that at the sweet spot $\Omega h^2 \sim 0.1$, the annihilation to Zh and coannihilation to ZW are comparable, indicating that the DM is a well-tempered bino/wino/Higgsino type.

In Table IV, we display the annihilation channels and scattering cross section of the DM candidate corresponding to the benchmark point in corresponding to the benchmark point in Table III. The relative values of the annihilation channels in Table IV are given at the time of freeze-out. We also obtained the annihilation channels in the zero velocity limit. The main annihilation channels relevant for indirect detection are $\tilde{\chi}_1^0\tilde{\chi}_1^0 \to Zh$ (90%), $\tilde{\chi}_1^0\tilde{\chi}_1^0 \to t\bar{t}$ (∼9%), and $\tilde{\chi}_1^0\tilde{\chi}_1^0 \to WW, ZZ$ ($\lesssim$1%). The absolute value of $\tilde{\chi}_1^0\tilde{\chi}_1^0 \to Zh$ in the zero velocity limit is $\langle\sigma v\rangle_{Zh} = 1.02 \times 10^{-26}$ cm^3 s^{-1}.

For the benchmark point, the spin-independent scattering cross section is 1.6×10^{-8} pb. We note that the scattering cross section for this $m_{\tilde{\chi}_1^0}$ is just at the exclusion limit at 90% C.L. from XENON100 [48]. Direct detection

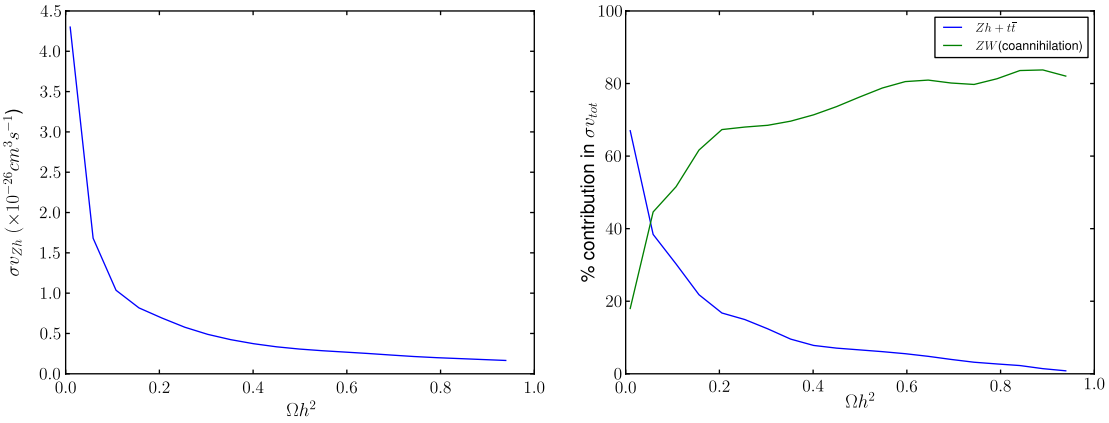

FIG. 4 (color online). Left panel: The annihilation cross section $\tilde{\chi}_1^0\tilde{\chi}_1^0 \to Zh$ as a function of the relic density for $\alpha = 1.5$ in the zero velocity limit. The cross section is large for large bino/Higgsino mixing. As the Higgsino becomes decoupled, the cross section for this annihilation channel becomes negligible. For a theoretical computation, we refer to Appendix A. Right panel: The relative importance of the $Zh + t\bar{t}$ channel and the ZW channel at freeze-out as a function of the relic density. For low relic density, the coannihilation channels $\tilde{\chi}_1^0\tilde{\chi}_2^0, \tilde{\chi}_1^0\tilde{\chi}_1^\pm \to ZW$ dominate. The DM is then a bino/wino well-tempered neutralino. For larger separation between bino and wino, the coannihilation becomes ineffective and the relic density increases as $\tilde{\chi}_1^0$ becomes predominantly bino. The main annihilation channel then becomes $\tilde{\chi}_1^0\tilde{\chi}_1^0 \to t\bar{t}$. For $\Omega h^2 \sim 0.1$, the annihilation to Zh and ZW are comparable.

bounds for well-tempered scenarios are getting particularly stringent. For $\mu > 0$, XENON100 exclusion limits force $m_{\tilde{\chi}_1^0} \gtrsim 600$ GeV in the large $\tan\beta$ limit [49]. Typically, bino/Higgsino mixing larger than 10% starts to conflict with exclusion bounds from XENON100 in these regions [50,51] (for our benchmark scenario, the degree of bino/Higgsino mixing is ~8%). We thus see that the $\tilde{B}/\tilde{H}/\tilde{W}$ well tempering is particularly interesting since it is likely to be conclusively probed by XENON1T [52]. In fact, by changing α, one can control the degree to which bino/wino coannihilation contributes to the relic density, and also the scattering cross section.

We note that the benchmark point ($M_{1/2} = 450$, $\mu = 670$ GeV) lies near the end of the lightest blue corridor bounded by the relic density constraint in Fig. 3. This benchmark point is now ruled out by LUX results [53], which exclude spin-independent scattering cross sections up to 6×10^{-9} pb and the entire lightest blue corridor up to this point is also ruled out, due to the fact that the Higgsino component in $\tilde{\chi}_1^0$ does not change appreciably. Higher values of $(M_{1/2}, \mu)$, leading to larger DM mass, are required to evade the direct detection constraints. Thus, light ($\lesssim$500 GeV) bino/wino/Higgsino DM in these models is ruled by current direct detection constraints. A higher mass can be easily obtained by increasing the values of $M_{1/2}$ and μ, while remaining within the relic density corridor bounded by the red lines in Fig. 3. We note that increasing

TABLE IV. Annihilation and spin-independent scattering cross sections at the benchmark point with $\tilde{B}/\tilde{H}/\tilde{W}$ DM. Only channels contributing greater than 1% to the total annihilation cross section at freeze-out are shown.

Annihilation cross section	$\tilde{\chi}_1^0\tilde{\chi}_1^0 \to Zh$	52%
	$\tilde{\chi}_1^0\tilde{\chi}_1^\pm \to ZW$	24%
	$\tilde{\chi}_1^0\tilde{\chi}_1^0 \to ZZ$	11%
	$\tilde{\chi}_1^0\tilde{\chi}_1^0 \to t\bar{t}$	6%
Scattering cross section (pb)	1.6×10^{-8}	

TABLE V. Spectrum at the benchmark point with $\tilde{B}/\tilde{W}$ DM.

GUT scale parameters	m_{16}	29 781	$M_{1/2}$	600	A_0	−60395	α	2.3
	m_{H_d}	40 724			m_{H_u}	35 237		
	$1/\alpha_G$	26.35	M_G	2.36×10^{16}	ϵ_3	0	λ	0.59
EW parameters	μ	1200			$\tan\beta$	49.65		
Fit	Total χ^2	1.72						
Spectrum	$m_{\tilde{u}}$	~29337	$m_{\tilde{d}}$	~29337	$m_{\tilde{e}}$	~29498		
	$m_{\tilde{t}_1}$	5832	$m_{\tilde{b}_1}$	8078	$m_{\tilde{\tau}_1}$	10 565	$M_{\tilde{g}}$	1135
	$m_{\tilde{\chi}_1^0}$	799.0	$m_{\tilde{\chi}_2^0}$	835.9	$m_{\tilde{\chi}_3^0}$	1201	$m_{\tilde{\chi}_4^0}$	1210
	$m_{\tilde{\chi}_1^+}$	835.5			$m_{\tilde{\chi}_1^+}$	1209		
	M_A	3093	$M_H^\pm$	3094	M_H	3131	M_h	123
DM	Ωh^2	0.099						
Gluino branching fractions	$g\tilde{\chi}_2^0$	55%	$g\tilde{\chi}_1^0$	31%	$tb\tilde{\chi}_1^\pm$	12%		

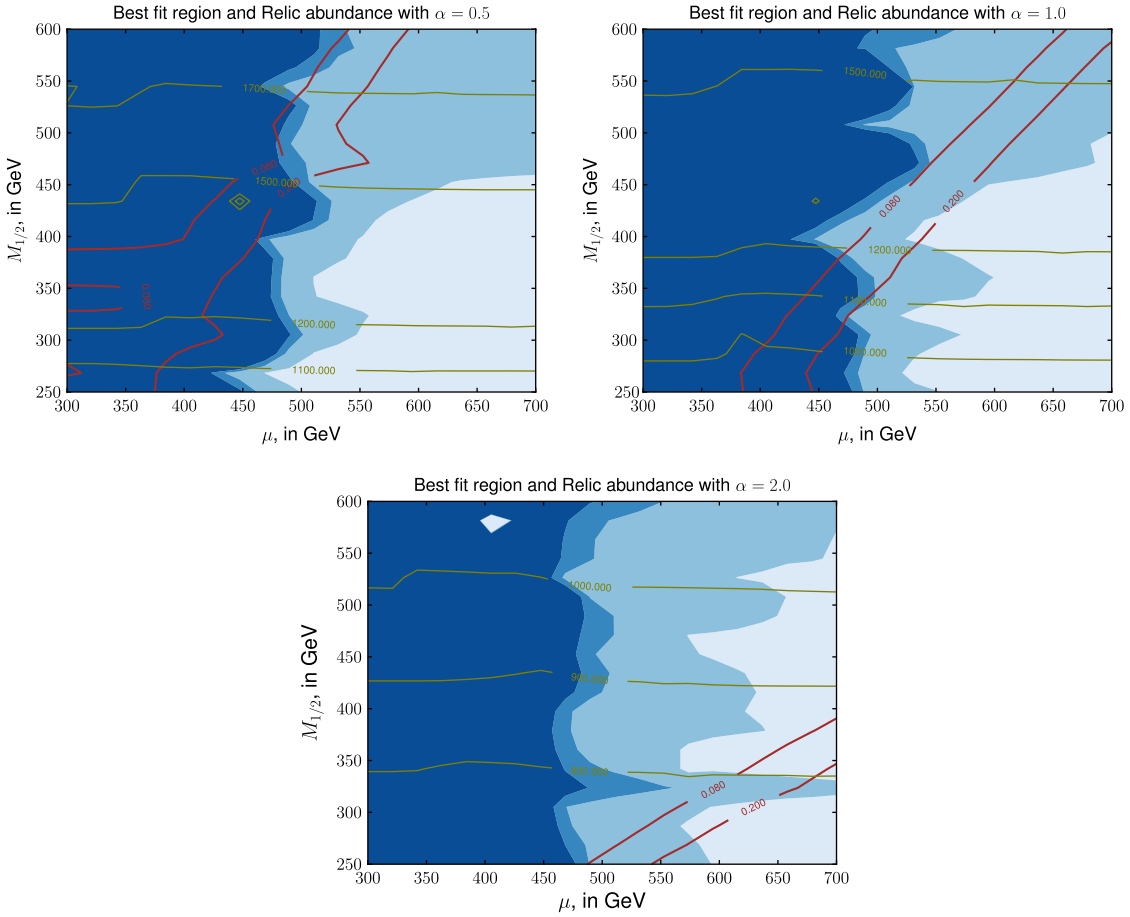

FIG. 5 (color online). Dependence on α: Best fit regions on a graph of $M_{1/2}$ versus μ in the case of $\alpha = 0.5$, 1, and 2. The region between the red lines gives $\Omega h^2 = 0.08 - 0.2$. The olive contours give the gluino mass. The blue contours (lightest to darkest) represent χ^2/d.o.f. $= 1$, 2.3, 3 corresponding to 95%, 90%, and 68% C.L., respectively. The figures show progressively better results as α is increased; the value of $\alpha = 1.5$ is shown in the main text as the benchmark point. The best fit is obtained for the case of $\alpha = 2$; however, the gluino mass is excluded in that case.

$M_{1/2}$ and μ in this way would remain within the low χ^2 region shown in lightest blue in Fig. 3, since the gluino mass would increase correspondingly.

We also note that outside the relic density corridor, various parts of parameter space (for example, the pure Higgsino parts with small μ and large $M_{1/2}$, or the pure bino part with the reverse) are allowed by direct detection constraints, since the scattering cross section for pure eigenstates is low. However, these parts are not physically interesting within the thermal DM framework where the relic density constraint must be critically satisfied.

D. Results for $\tilde{B}/\tilde{W}$ DM

As α increases further, the wino starts becoming a substantial component of the LSP and the relic abundance is satisfied for larger values of μ. In this region we obtain a $\tilde{B}/\tilde{W}$ DM. A typical spectrum is shown in Table V. Note that we have chosen a higher scale for the supersymmetric scalar masses, m_{16}, so as to obtain a better fit to the Higgs mass. This also gives rise to larger corrections to the gluino mass. The gluino is $\gtrsim$1100 GeV, in spite of $\alpha > 2$, in comparison with Fig. 5, where m_{16} was chosen to be 20 TeV. The other qualitative features of the spectrum remain unchanged. The main channels as well as the spin-independent scattering cross section are shown in Table VI. The annihilation cross section of the DM is dominated by various coannihilation processes among $\tilde{\chi}_1^0$, $\tilde{\chi}_2^0$, and $\tilde{\chi}_1^\pm$. The spin-independent scattering cross section is well below

TABLE VI. Annihilation and spin-independent (SI) scattering cross sections at the benchmark point with $\tilde{B}/\tilde{W}$ DM. Only channels contributing greater than 1% to the total annihilation cross section are shown.

Annihilation cross section	$\tilde{\chi}_1^0\tilde{\chi}_1^0 \to Zh$	6%
	$\tilde{\chi}_1^0\tilde{\chi}_1^\pm \to ZW, Wh$	24%
	$\tilde{\chi}_2^0\tilde{\chi}_1^\pm \to ff, ZW$	32%
	$\tilde{\chi}_2^0\tilde{\chi}_2^0 \to WW$	4%
	$\tilde{\chi}_1^\pm\tilde{\chi}_1^\pm \to WW, ZZ, ff$	21%
SI scattering cross section (pb)	3.5×10^{-9}	

XENON100 limits, as expected in this case. The spin-independent scattering cross section is below current bounds from LUX.

V. COLLIDER BOUNDS

Good fits to all the observables (especially the Higgs boson mass) require the gluino to light and it is the most favorable to be probed at the LHC. The main decay modes of the gluino are three-body decays into $t\bar{t}\tilde{\chi}^0_{(1,2)}$, $tb\tilde{\chi}^{\pm}$, $b\bar{b}\tilde{\chi}^0_{(1,2)}$; mediated by the third family scalars: the top squarks and the sbottoms. In addition, the loop decay of the gluino ($\tilde{g} \to g\tilde{\chi}^0$) also occurs with significant branching ratios when the scalars become heavier. This is especially apparent in the $\tilde{B}/\tilde{W}$ benchmark point in Table V. All the decay modes of the gluino lead to large missing energy signatures and multiple jets with large p_T. In addition, the three-body decays will lead to b jets in the final state. Gluino pair production at the LHC and the subsequent decay of the gluino into $t\bar{t}\tilde{\chi}^0_{(1,2)}$, $tb\tilde{\chi}^{\pm}$ yield the background-free same-sign dilepton signatures. The ATLAS and CMS Collaborations have analyzed the 20 fb^{-1} of data from the LHC at 8 TeV in many different channels [29,54–59] and interpreted them as constraints on the gluino in simplified model scenarios when the gluino decays into a single decay mode 100% of the time. Depending on the simplified scenario, the analyses rule out gluinos between 1100 and 1300 GeV.

Existing LHC data were reinterpreted in the context of minimal Yukawa unified SUSY models in Ref. [60]. The spectrum discussed here is different from minimal Yukawa unified GUTs in the gaugino sector. The other main features of the spectrum like heavy scalars and lighter third-generation scalars remain the same in both cases. In both cases, the gluino decays into multiple final states and the loop decays of the gluino had a significant branching ratio. We expect the results obtained there to be applicable to the spectrum presented here. Since the mass difference between the gluino and the electroweakinos is smaller here than in the universal scenarios, the bounds, if at all any different, will be slightly weaker. In Ref. [60], benchmark points with varying gluino masses were tested against three CMS analyses [29,55,61]. The nonsimplified decays of the gluino and considerable decay into $g\tilde{\chi}^0$ (which produce fewer jets, no b jets and no leptons) made the bounds on the gluinos in these models weaker by about 20% compared to the limits on simplified scenarios. For the benchmark scenarios we have studied here, we expect the current data from LHC to rule out gluinos below 1000 GeV.

The ATLAS and CMS Collaborations have also analyzed the 20 fb^{-1} data to constrain the production cross sections of the electroweakinos [62–65]. The lower bound on the chargino is about 350 GeV when the chargino decays into a massless LSP and an on-shell W boson. The bounds become weaker as the mass difference between chargino and the LSP decreases below the W-mass scale, so that the chargino decays via a virtual W. In the scenarios presented here, the LSP is 474 GeV, the mass difference between the chargino and the LSP is 80 GeV in the $\tilde{B}/\tilde{W}/\tilde{H}$, and the LSP is 800 GeV and is about 35 GeV lighter than the chargino in the $\tilde{B}/\tilde{W}$ case. The mirage pattern naturally compresses the gaugino spectrum and in order to evade the gluino bounds the scale of the electroweakinos is much higher than in universal gaugino mass models. Thus, the most viable particle to look for in the colliders is the gluino, and the electroweakinos will remain beyond the reach of the LHC. The 14 TeV LHC after collecting about 300 fb^{-1} of data has a discovery potential for gluinos with mass $\lesssim$1.9 TeV [66,67]. Therefore, the benchmark scenarios presented here will be conclusively tested by the 14 TeV LHC.

VI. COMMENTS AND SUMMARY

In this work, we have investigated the interplay between four physics components within the context of Yukawa unified supersymmetric GUTS.

(i) Thermal relic abundance.
(ii) Low-energy observables including fermion masses and flavor.
(iii) 125 GeV Higgs mass.
(iv) Collider bounds on the gluinos.

We have studied the viability of a thermal DM candidate in Yukawa unified SUSY GUTS. Given the model parameters at the GUT scale, we have used the low-energy observables M_W, M_Z, G_F, $\alpha_{\rm em}^{-1}$, $\alpha_s(M_Z)$, M_t, $m_b(m_b)$, M_τ, $b \to s\gamma$, BR($B_s \to \mu^+\mu^-$)and M_h to constrain the parameter space. It is well known that uniformly heavy scalars and decoupled SUSY Higgs sector are required in these models to evade flavor physics constraints from $b \to s\gamma$, BR($B_s \to \mu^+\mu^-$). The heavy scalars make it impossible to achieve coannihilation scenarios with staus or the CP-odd Higgs. The model also prefers a light gaugino spectrum and therefore disfavors Higgsino LSP. Then, the remaining option to obtain a thermal DM candidate in these models is to consider a well-tempered neutralino that is either $\tilde{B}/\tilde{H}$ or $\tilde{B}/\tilde{W}$ or $\tilde{B}/\tilde{H}/\tilde{W}$ admixture.

The first observation is that light Higgsinos with mass $\lesssim\mathcal{O}(500)$ GeV are difficult to obtain in these models. In particular, the tension arises from simultaneously obtaining acceptable corrections to the bottom quark mass and the mass of the Higgs, as well as evading the lower bound on the mass of the gluino mass. This is clearly represented in Fig. 1, where Higgsino masses less than $\tilde{\mathcal{O}}(500)$ GeV uniformly have a large χ^2/d.o.f. for gluino mass $\gtrsim$1100 GeV. This makes light well-tempered $\tilde{B}/\tilde{H}$ DM less preferred and, hence, universal gaugino masses at the GUT scale also less preferred, since $\tilde{B}/\tilde{H}$ DM is the only well-tempered option with that boundary condition.

We studied the cases of $\tilde{B}/\tilde{H}/\tilde{W}$ and $\tilde{B}/\tilde{W}$ DM by allowing for nonuniversal gaugino masses at the GUT

scale, in a mirage pattern. Nonuniversality of the gauginos at the GUT scale is required to compress the mass splitting between the bino and the wino. We find that there are small regions of parameter space that can accommodate all the low-energy observables including a 125 GeV Higgs that do not conflict with the LHC constraints on the gluino. In both cases there is a considerable degree of fine-tuning between the Higgsino, third-generation squark, and gluino masses in order to satisfy all the constraints.

The best fit regions require a light gluino. The lower bound on the gluino mass is growing from the LHC data and the 14 TeV run at the LHC will conclusively test the regions discussed here. For gluino ~ 1.3 TeV, we find tensions in obtaining a 125 GeV Higgs mass, in spite of the heavy scalars in the model. Our findings are that the trilinear coupling A_t is pushed beyond maximal mixing, and hence drives the Higgs mass to smaller values. On the other hand, the $\tilde{B}/\tilde{H}/\tilde{W}$ will also be probed by XENON1T. While there are still small pockets of the parameter space with accidental degeneracies, we find that these are considerably fine-tuned and may even require DM with mass larger than a TeV. It is important to note that independent of the thermal dark matter viability, these models will be severely constrained by the absence of a gluino at the next run of the LHC. Hints of the gluino at the next run of the LHC without any immediate detection from direct DM searches would leave only the $\tilde{B}/\tilde{W}$ as a viable scenario.

ACKNOWLEDGMENTS

We would like to thank Stuart Raby for helpful discussions, and Radovan Dermisek for the code MATON which has been adapted to do a major portion of the top-down analysis. We also acknowledge discussions with Genevieve Belanger, Alexander Pukhov, and Paolo Gondolo. K. S. is supported by NASA Astrophysics Theory Grant No. NNH12ZDA001N. A. A. is partially supported by DOE Grant No. DOE/ER/01545-901.

APPENDIX A: ANNIHILATION CHANNEL $\tilde{\chi}_1^0\tilde{\chi}_1^0 \to Zh$

In this section, we present the analytical expression for the annihilation cross section of DM into Zh final states, following [68]. The annihilation of DM into Zh final state occurs due to two contributions: s-channel exchange of a Z and t- and u-channel exchange of all four neutralinos. The cross section in the limit of $v_{\rm rel} \to 0$ is given by

$$\sigma_{Zh} v_{\rm rel} = \frac{k X_{Zh}}{32\pi m_{\tilde{\chi}_1^0}^3}, \tag{A1}$$

where

$$k = \left[m_{\tilde{\chi}_1^0}^2 - \frac{1}{2}(m_Z^2 + m_h^2) + \frac{(m_Z^2 - m_h^2)^2}{16 m_{\tilde{\chi}_1^0}^2} \right]^{1/2} \tag{A2}$$

is the momentum of the outgoing particles. In the limit of heavy Higgs partners, the quantity X is given by

$$X_{Zh} = 2k^2 \frac{m_{\tilde{\chi}_1^0}^2}{m_Z^2} \left[\frac{z F_{nn}}{m_Z^2} + \sum\nolimits_K \frac{2 g M_{2nk} F_{nk} (m_{\tilde{\chi}_k^0} - m_{\tilde{\chi}_1^0})}{t - m_{\tilde{\chi}_k^0}^2} \right]^2. \tag{A3}$$

The various quantities in (A3) are (i) the coupling at the hZZ vertex $z = g m_Z \sin\beta - \alpha/\cos\theta_W$ [g is the $SU(2)_L$ coupling constant], (ii) the coupling of the $Z\tilde{\chi}_i^0\tilde{\chi}_j^0$ vertex $F_{ij} = g(Z_{i3}Z_{j3} - Z_{i4}Z_{j4})/2\cos\theta_W$, (iii) the coupling at the $H_i^0\tilde{\chi}_j^0\tilde{\chi}_k^0$ vertex M_{ijk} available in [69], and (iv) $t = \frac{m_Z^2 - m_h^2}{2} - m_{\tilde{\chi}_1^0}^2$. The sum is over all neutralinos.

APPENDIX B: $\alpha = 0.5$, 1 AND 2

In the main text, we have given the examples of $\alpha = 0$ (universal gaugino masses) and $\alpha = 1.5$. The problems with the universal gaugino mass case were described, and the eventual benchmark at $\alpha = 1.5$ was presented. In this Appendix, we give the results for several intermediate values of α. We note that the region with relic density $\Omega h^2 = 0.08$–0.2 starts extending more and more into the region with small χ^2, as the b-mass fitting improves due to the reasons mentioned in the text. For $\alpha = 2.0$, the χ^2 fit is the best; however, the tradeoff is that the gluino becomes too light.

[1] S. Dimopoulos, S. Raby, and F. Wilczek, Phys. Rev. D **24**, 1681 (1981).
[2] S. Dimopoulos and H. Georgi, Nucl. Phys. **B193**, 150 (1981).
[3] L. E. Ibanez and G. G. Ross, Phys. Lett. **105B**, 439 (1981).
[4] N. Sakai, Z. Phys. C **11**, 153 (1981).
[5] M. Einhorn and D. Jones, Nucl. Phys. **B196**, 475 (1982).
[6] W. J. Marciano and G. Senjanovic, Phys. Rev. D **25**, 3092 (1982).
[7] T. Blazek, R. Dermisek, and S. Raby, Phys. Rev. Lett. **88**, 111804 (2002).
[8] H. Baer and J. Ferrandis, Phys. Rev. Lett. **87**, 211803 (2001).
[9] T. Blazek, R. Dermisek, and S. Raby, Phys. Rev. D **65**, 115004 (2002).

[10] K. Tobe and J. D. Wells, Nucl. Phys. **B663**, 123 (2003).
[11] D. Auto, H. Baer, C. Balázs, A. Belyaev, J. Ferrandis, and X. Tata, J. High Energy Phys. 06 (2003) 023.
[12] I. Gogoladze, Q. Shafi, and C. S. Un, Phys. Lett. B **704**, 201 (2011).
[13] I. Gogoladze, Q. Shafi, and C. S. Un, J. High Energy Phys. 08 (2012) 028.
[14] M. Badziak, M. Olechowski, and S. Pokorski, J. High Energy Phys. 08 (2011) 147.
[15] A. Anandakrishnan, S. Raby, and A. Wingerter, arXiv:1212.0542.
[16] A. Anandakrishnan and S. Raby, arXiv:1303.5125.
[17] M. Adeel Ajaib, I. Gogoladze, Q. Shafi, and C. S. Un, arXiv:1303.6964.
[18] T. Moroi and L. Randall, Nucl. Phys. **B570**, 455 (2000).
[19] R. Allahverdi, B. Dutta, and K. Sinha, Phys. Rev. D **87**, 075024 (2013).
[20] R. Allahverdi, M. Cicoli, B. Dutta, and K. Sinha, arXiv:1307.5086.
[21] R. Allahverdi, B. Dutta, and K. Sinha, Phys. Rev. D **86**, 095016 (2012).
[22] H. Baer and H. Summy, Phys. Lett. B **666**, 5 (2008).
[23] H. Baer, M. Haider, S. Kraml, S. Sekmen, and H. Summy, J. Cosmol. Astropart. Phys. 02 (2009) 002.
[24] R. Dermisek, S. Raby, L. Roszkowski, and R. Ruiz De Austri, J. High Energy Phys. 04 (2003) 037.
[25] R. Dermisek, S. Raby, L. Roszkowski, and R. Ruiz de Austri, J. High Energy Phys. 09 (2005) 029.
[26] H. Baer, S. Kraml, S. Sekmen, and H. Summy, J. High Energy Phys. 03 (2008) 056.
[27] N. Arkani-Hamed, A. Delgado, and G. Giudice, Nucl. Phys. **B741**, 108 (2006).
[28] Technical Report No. ATLAS-CONF-2013-061, CERN, 2013.
[29] S. Chatrchyan *et al.* (CMS Collaboration), arXiv:1305.2390.
[30] S. Chatrchyan *et al.* (CMS Collaboration), Phys. Lett. B **716**, 30 (2012).
[31] G. Aad *et al.* (ATLAS Collaboration), Phys. Lett. B **716**, 1 (2012).
[32] K. Choi and H. P. Nilles, J. High Energy Phys. 04 (2007) 006.
[33] V. Lowen and H. P. Nilles, Phys. Rev. D **77**, 106007 (2008).
[34] H. Baer, E.-K. Park, X. Tata, and T. T. Wang, Phys. Lett. B **641**, 447 (2006).
[35] T. Blazek, S. Raby, and S. Pokorski, Phys. Rev. D **52**, 4151 (1995).
[36] N. Bernal, A. Djouadi, and P. Slavich, J. High Energy Phys. 07 (2007) 016.
[37] A. Crivellin *et al.*, arXiv:1203.5023.
[38] G. Belanger, F. Boudjema, A. Pukhov, and A. Semenov, Nuovo Cimento Soc. Ital. Fis. C N2 **033**, 111 (2010).
[39] F. James and M. Roos, Comput. Phys. Commun. **10**, 343 (1975).
[40] Heavy Flavor Averaging Group, http://www.slac.stanford.edu/xorg/hfag/, 2012.
[41] J. Beringer *et al.* (Particle Data Group), Phys. Rev. D **86**, 010001 (2012).
[42] R. Aaij *et al.* (LHCb Collaboration), arXiv:1211.2674.
[43] P. Ade *et al.* (Planck Collaboration), arXiv:1303.5062.
[44] L. Roszkowski, R. Ruiz de Austri, R. Trotta, Y.-L. S. Tsai, and T. A. Varley, Phys. Rev. D **83**, 015014 (2011).
[45] K. Kowalska, L. Roszkowski, and E. M. Sessolo, J. High Energy Phys. 06 (2013) 078.
[46] M. Guchait, D. Roy, and D. Sengupta, Phys. Rev. D **85**, 035024 (2012).
[47] S. Raby, M. Ratz, and K. Schmidt-Hoberg, Phys. Lett. B **687**, 342 (2010).
[48] E. Aprile *et al.* (XENON100 Collaboration), Phys. Rev. Lett. **109**, 181301 (2012).
[49] C. Cheung, L. J. Hall, D. Pinner, and J. T. Ruderman, arXiv:1211.4873.
[50] B. Dutta, T. Kamon, N. Kolev, K. Sinha, K. Wang, and S. Wu, Phys. Rev. D **87**, 095007 (2013).
[51] T. Han, Z. Liu, and A. Natarajan, arXiv:1303.3040.
[52] E. Aprile (XENON1T Collaboration), arXiv:1206.6288.
[53] D. Akerib *et al.* (LUX Collaboration), arXiv:1310.8214.
[54] S. Chatrchyan *et al.* (CMS Collaboration), arXiv:1311.6736.
[55] S. Chatrchyan *et al.* (CMS Collaboration), arXiv:1303.2985.
[56] G. Aad *et al.* (ATLAS Collaboration),J. High Energy Phys. 10 (2013) 130.
[57] Technical Report No. ATLAS-CONF-2013-089, CERN, 2013.
[58] Technical Report No. ATLAS-CONF-2013-062, CERN, 2013.
[59] Technical Report No. ATLAS-CONF-2013-047, CERN, 2013.
[60] A. Anandakrishnan, B. C. Bryant, S. Raby, and A. Wingerter, arXiv:1307.7723.
[61] S. Chatrchyan *et al.* (CMS Collaboration), J. High Energy Phys. 03 (2013) 037.
[62] CMS Collaboration, Technical Report No. CMS-PAS-SUS-13-017, CERN, 2013.
[63] CMS Collaboration, Technical Report No. CMS-PAS-SUS-13-006, CERN, 2013.
[64] Technical Report No. ATLAS-CONF-2013-093, CERN, 2013.
[65] ATLAS Collaboration, Technical Report No. ATLAS-CONF-2013-035, CERN, 2013.
[66] H. Baer, V. Barger, A. Lessa, and X. Tata, Phys. Rev. D **86**, 117701 (2012).
[67] CMS Collaboration, arXiv:1307.7135.
[68] M. Kamionkowski, Phys. Rev. D **44**, 3021 (1991).
[69] K. Griest, M. Kamionkowski, and M. S. Turner, Phys. Rev. D **41**, 3565 (1990).